Journal of Hazardous Materials 192 (2011) 1697–1704

Contents lists available at ScienceDirect

Journal of Hazardous Materials

journal homepage: www.elsevier.com/locate/jhazmat

The degradation of 1,2,4-trichlorobenzene using synthesized Co_3O_4 and the hypothesized mechanism

Shijing Lin[a,b], Guijin Su[a,*], Minghui Zheng[a], Manke Jia[a], Chuansong Qi[b], Wei Li[b]

[a] State Key Laboratory of Environmental Chemistry and Ecotoxicology, Research Center for Eco-Environmental Sciences, Chinese Academy of Sciences, P.O. Box 2871, Beijing 100085, China
[b] Department of Chemical Engineering, Beijing Institute of Petrochemical Technology, Beijing 102617, China

ARTICLE INFO

Article history:
Received 26 November 2010
Received in revised form 30 May 2011
Accepted 2 July 2011
Available online 8 July 2011

Keywords:
Co_3O_4
Different morphologies
Degradation
1,2,4-trichlorobenzene
Mechanism

ABSTRACT

Co_3O_4 was synthesized with cabbage-like, plate-like and sphere-like morphologies. The effect of different morphologies on the degradation of 1,2,4-trichlorobenzene (1,2,4-TrCB) was evaluated, and the cabbage-like Co_3O_4 exhibited the highest reactivity. The degradation of 1,2,4-TrCB on the cabbage-like Co_3O_4 is hypothesized to act competitively via hydrodechlorination and oxygen-attacking pathways. By the hydrodechlorination pathway, 1,2,4-TrCB is successively dechlorinated into the three dichlorobenzenes (DCBs) and then monochlorobenzene (MCB). The yield of the DCBs was in the order of *p*-DCB > *m*-DCB > *o*-DCB, which can be explained by the calculated C–Cl bond dissociation energies in 1,2,4-TrCB and DCBs. Derivatization and electron spin resonance experiments identified that lattice oxygen and superoxide anions may take part in the oxidation pathway. The lattice oxygen initiated a partial oxidation of 1,2,4-TrCB, leading to the formation of chlorinated phenols. The superoxide anions caused ring-cracking oxidation of 1,2,4-TrCB, possibly producing some low-molecular-weight products, thus explaining a mass imbalance in the chlorine atoms and total organic carbon.

1. Introduction

Chlorinated aromatic compounds are ubiquitous pollutants, which have been found in most environmental media including sediment, soil and water [1,2]. They are often highly toxic, recalcitrant to degradation, and may bioaccumulate through the food chain. Once present in the environment, they can cause tremendous harm to human health and the environment. Thus, the control of chlorinated aromatic pollution is a matter of public concern.

Chlorinated benzenes (CBz), of which there are 12 possible congeners, are a major group of chlorinated aromatics, and many are on the USEPA priority pollutants list [3]. They have been widely used in industrial, agricultural and domestic products including pesticides, soil fumigants, disinfectants, toilet deodorants, solvents, and as precursors for the production of dyes and silicone coatings [4,5]. When chlorinated benzenes are released into the environment, they can be transformed to more toxic polychlorinated dibenzo-p-dioxins and dibenzofurans (PCDD/Fs), which are highly carcinogenic and mutagenic [6]. Owing to their structure and environmental hazard, chlorinated benzenes have often been used as model pollutants when exploring efficient treatment technologies for chlorinated aromatics and identifying the degradation mechanisms.

Metal oxide catalysts have attracted attention for the degradation of CBz, due to their relatively low costs, high catalytic activity and thermal stability, and the ease of preparation of high surface area materials [7–17]. The decomposition of hexachlorobenzene (HCB) has been carried out over various metal oxides (i.e., MgO, CaO, BaO, La_2O_3, CeO_2, MnO_2, Fe_2O_3, and Co_3O_4) supported on Al_2O_3 [16]. For most of the metal oxide catalysts, the dechlorination efficiency exceeded 94.2% after treatment at 300 °C for 60 min. Jia et al. developed a flower-like Fe_3O_4 with a high surface area, which has much higher activity than the commercial Fe_3O_4, to degrade HCB at 300 °C [17]. For these and similar reactions [11,16,17], a series of less chlorinated benzenes have been identified as the degradation products, leading to agreement about the presence of a sequential hydrodechlorination pathway. However, little work has been done to elucidate the driving force underlying the hydrodechlorination pathway.

Oxidative degradation has also been identified as a pathway for the degradation of CBz over metal oxides. Partial oxidation intermediates (i.e., phenolates, acetates and formates) have been identified during the degradation of hexachlorobenzene over a composite Ca–Fe oxide [18], and during the degradation of 1,2-dichlorobenzene over supported Cr_2O_3, V_2O_5, MoO_3, Fe_2O_3, and Co_3O_4 [19]. These intermediates can decompose further to CO, CO_2, and H_2O. Reactive oxygen species (ROS) such as $O_2^{-\bullet}$, and $^\bullet OH$ are strong oxidants, which can oxidize organic compounds to smaller molecular intermediates or to CO_2 and H_2O [20,21]. However, there

* Corresponding author. Tel.: +86 10 62849356; fax: +86 10 62923563.
E-mail address: gjsu@rcees.ac.cn (G. Su).

0304-3894/$ – see front matter © 2011 Elsevier B.V. All rights reserved.
doi:10.1016/j.jhazmat.2011.07.008

have been few reports to indicate which ROS might be involved in the oxidative degradation of CBz over metal oxides.

Of the metal oxides, magnetic Co_3O_4 with a spinel structure has been identified as a preferential catalyst for environmental protection [22,23]. Co_3O_4 has been prepared with a range of different morphologies including nanospheres, nanocubes, nanofibers, and mesoporous structures [24–28]. The properties of these synthesized metal oxides are strongly dependent on their morphologies, which determine the structural properties such as crystalline quality, particle size and surface area. Therefore, evaluating the effect of different morphologies on the ability of Co_3O_4 to degrade CBz is very significant.

In recent years, a simple and economic ethylene glycol mediated process has been developed to construct novel metal oxide materials [11,17,29–33]. The prepared materials are often hierarchically composed of nanosized building blocks, while the size of the overall structure is at the micrometer scale. This hierarchical structure can maintain a high catalytic activity, as it is constructed of interconnected nanoparticles. Also, due to the micrometer size of the overall particle, it can also effectively inhibit aggregation, and the separation and recycling of the metal oxide material is easier than for pure nanoparticles. However, there are currently no reports on the degradation of chlorinated aromatics using micrometer-sized nanostructured Co_3O_4.

In this paper, Co_3O_4 was synthesized with three different morphological structures by the ethylene glycol mediated reaction, to degrade 1,2,4-trichlorobenzene (1,2,4-TrCB). The three structures have been described as sphere-like, plate-like, and cabbage-like structures (the cabbage-like structure consists of many layers of distorted nanoplates stacked together, giving the whole structure a "cabbage-like" appearance). The effect of the different morphological structures on the degradation of 1,2,4-TrCB was evaluated, and the degradation products were identified by GC–MS. The likely hydrodechlorination pathway was elucidated by a theoretical calculation of the C–Cl bond dissociation energies (BDEs) in 1,2,4-TrCB and DCBs. Electron spin resonance (ESR) experiments were used to study the role of reactive oxygen species in the degradation of 1,2,4-TrCB.

2. Experimental

2.1. Preparation and characterization of Co_3O_4 with different morphologies

Commercial Co_3O_4 was purchased from Beijing Chemical Reagent Ltd. and used as received.

The prepared Co_3O_4 was synthesized using an ethylene glycol (EG) mediated reaction. The preparation was adopted from Wan et al. with minor modification [33]. In a typical synthesis reaction, $Co(CH_3COO)_2{\cdot}4H_2O$ (Beijing Chemical Reagent Ltd.) and Polyvinylpyrrolidone (PVP, Mw = 58,000, ACROS Organics) were added to ethylene glycol (Beijing Chemical Reagent Ltd.). The mixture was stirred with a magnetic stir bar and heated to 170 °C under nitrogen for various lengths of time. The precipitated Co_3O_4 precursor was collected and washed three times with absolute alcohol using centrifugation–redispersion cycles, and then calcined at 400 °C for 2 h to prepare the Co_3O_4. By changing the reactant concentrations and the heating time, Co_3O_4 with three different morphologies, described as sphere-like, plate-like and cabbage-like, was synthesized.

The morphology of the products was characterized using scanning electron microscopy (HRSEM, Zeiss supra 55), transmission electron microscopy (HRTEM, JEM-2100 electron microscope, JEOL), X-ray powder diffraction (XRD, 7000 diffractometer with CuKα, λ = 0.15418 nm), and the Brunauer–Emmett–Teller (BET) analysis (ASAP 2020) and Automated Surface Area & Pore Size Analyzer.

2.2. Degradation experiments

The degradation experiments were carried out in small glass ampoules, 10 cm long and 0.4 cm i.d. Typically, 1.5 μL of 1,2,4-TrCB (11954 nmol) was mixed with a known amount of Co_3O_4 in the ampoule which was then sealed under the air atmosphere and heated in an oven. The reaction condition was set at 200–300 °C for 60 min. To ensure the repeatability of the experiments, all experiments were performed in triplicate, with a relative standard deviation (RSD) of parallel experiments of less than 5%.

The sample analysis is described in detail elsewhere and briefly summarized here [12,34]. On completion of the reactions, the glass ampoules were carefully crushed and extracted three times with hexane (15 mL) for 15–20 min each time in an ultrasonic extractor. The solution was then washed three times with 10 mL water. The aqueous and hexane layers were separated. The inorganic Cl^- in the recovered water was measured by ion chromatograph (792 Basic IC, Metrohm Ltd., Herisain, Switzerland). The hexane layers were combined and dried with anhydrous sodium sulfate, and analyzed for CBz using an Aglient 6890 gas chromatograph equipped with a HP-5MS capillary column (30 m length, 0.25 mm i.d., 0.25 μm film thickness) and interfaced to an Agilent 5973N MSD (Agilent Technologies, USA). Quantitative analyses of the CBz were performed in selected ion monitoring mode using the two most abundant molecular ion clusters. The degradation efficiency (DE) was calculated using the following equation:

$$\mathrm{DE}\ (\%) = \left(\frac{1 - R_{\mathrm{TrCB}}}{I_{\mathrm{TrCB}}}\right) \times 100\% \quad (1)$$

where I_{TrCB} is the initial number of moles of 1,2,4-TrCB, and R_{TrCB} is the number of moles of 1,2,4-TrCB after the reaction.

2.3. Theoretical calculations

All theoretical calculations were carried out using the Gaussian 03 program, with fully optimized geometries of 1,2,4-TrCB and DCBs. The C–Cl BDEs in 1,2,4-TrCB and DCBs, and the energy difference of single molecule relative to *p*-DCB were calculated by the density functional theory (DFT) method at the B3LYP/6-311++G** theory level.

2.4. Total organic carbon (TOC) analysis

TOC content of the sample was analyzed on a solid TOC analyzer (O.I. Analyzer, College Station, TX, USA) using a high-temperature combustion method. The experimental details are described elsewhere [35]. After reaction between 1.5 μL 1,2,4-TrCB and 100 mg of cabbage-like Co_3O_4 at 300 °C for 60 min, the samples were loaded into the combustion cup which was packed with quartz wool. The samples were flashed at 900 °C for 6 min in the combustion house, and the signal was detected by non-dispersed infrared (NDIR) detection. The TOC of the starting materials (unreacted samples) were also analyzed under the same conditions to allow comparisons.

2.5. Derivatization experiments

To confirm whether phenolate species were produced during the degradation of 1,2,4-TrCB, derivatization experiments were conducted. 1,2,4-TrCB (1.5 μL) was reacted with 100 mg of cabbage-like Co_3O_4 at 300 °C for 60 min. The reaction products

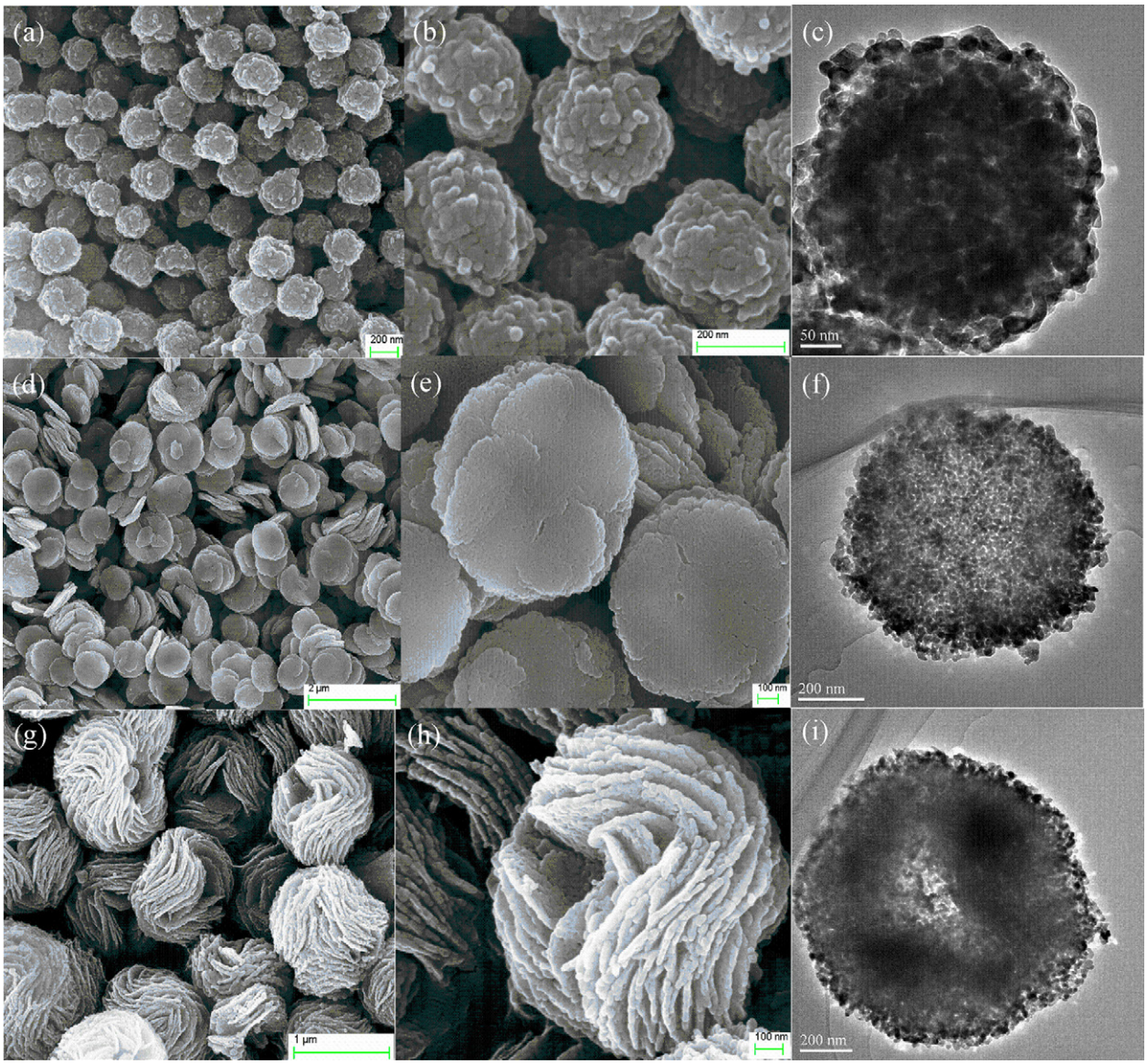

Fig. 1. (a, b) HRSEM images and (c) HRTEM image of sphere-like Co_3O_4; (d, e) HRSEM images and (f) HRTEM image of plate-like Co_3O_4; (g, h) HRSEM images and (i) HRTEM image of cabbage-like Co_3O_4.

were derivatized in water using acetic anhydride and then analyzed by GC–MS.

2.6. ESR experiments

The superoxide anions were measured using an electron spin resonance analyzer (ESR, ESP 300E, Bruker) as described below. 100 mg of cabbage-like Co_3O_4 and 1.5 μL 1,2,4-TrCB were reacted at 300 °C for 60 min. The resulting product was immediately dissolved in dimethylsulfoxide (DMSO, Sigma Chemical Co.). The superoxide anions were characterized by ESR using 5,5-dimethyl-1-pyrroline-N-oxide (DMPO, Sigma Chemical Co.) as the spin trapping agent. The instrument settings were: microwave power at 10 mW; microwave frequency at 9.8 GHz; scan range at 100 G; modulation frequency at 100 kHz; modulation amplitude at 2 G; and sweep time at 41.943 s. To measure the hydroxyl radical, the only difference was the use of water as the solvent instead of DMSO. A reaction using the cabbage-like Co_3O_4 but without 1,2,4-TrCB was also measured by the ESR experiments under the same conditions for comparison.

3. Results and discussion

3.1. Characterization of Co_3O_4

The morphologies of the synthesized Co_3O_4 were regulated by controlling the initial concentration of $Co(CH_3COO)_2{\cdot}4H_2O$ and the heating time. When the EG solution contained 50 mM $Co(CH_3COO)_2{\cdot}4H_2O$ and 0.23 mM PVP, and was heated at 170 °C for 40 min, a sphere-like product with a diameter approximately 0.25 μm was obtained (Fig. 1(a–c)). When the concentration of $Co(CH_3COO)_2{\cdot}4H_2O$ was increased to 90 mM, and the heating time was 35 min, the morphology of the product changed from spheres to round nanoplates with diameters of approximately 0.7 μm, as shown in Fig. 1(d–f). Finally, when the concentration of $Co(CH_3COO)_2{\cdot}4H_2O$ was increased to 93 mM with a heating time of 45 min, the plates became severely distorted and many layers of the distorted nanoplates stacked together, forming an overall structure with a "cabbage-like" morphology and a diameter of approximately 1 μm (Fig. 1(g–i)). The high-resolution TEM images in Fig. 1 show that all three structures are constructed of intercon-

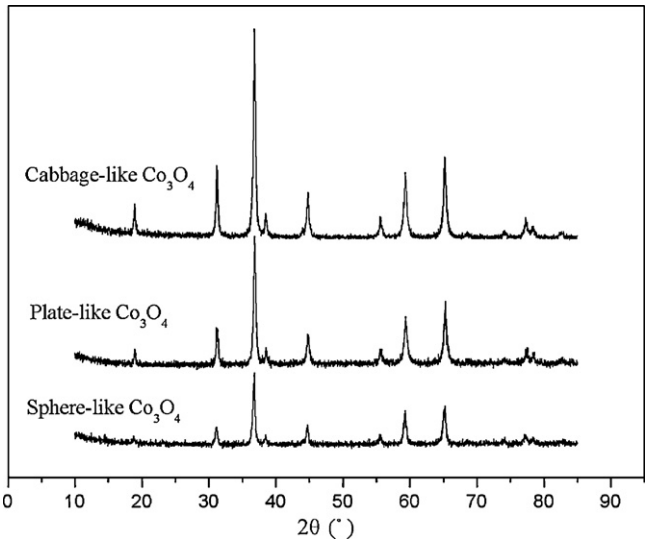

Fig. 2. XRD patterns of the prepared Co_3O_4.

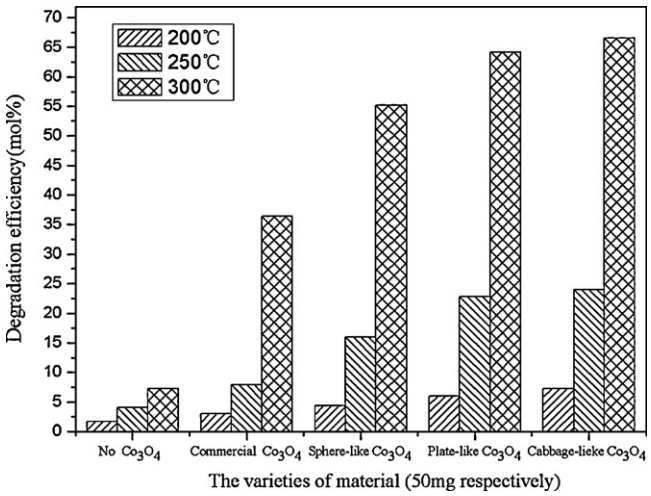

Fig. 3. Effect of Co_3O_4 with different morphologies on the degradation of 1,2,4-TrCB under different reaction temperatures.

nected nanoparticles less than 20 nm in size, making the samples porous. In comparison, the commercial Co_3O_4 appeared as aggregated irregular particles (SEM image of commercial Co_3O_4 is shown in Fig. S1 of the Supplementary Material).

The X-ray powder diffraction (XRD) patterns shown in Fig. 2 show that all the products with varying morphologies were identified as being consistent with cubic symmetry Co_3O_4 (JCPDS No. 78-1969). These results confirm that micrometer-sized nanostructured Co_3O_4 with three different morphologies was successfully prepared by the EG mediated process.

Nitrogen adsorption isotherms determined the BET surface area and total pore volume of the Co_3O_4 with different morphologies, as shown in Table 1. The BET surface areas of the sphere-like, plate-like and cabbage-like Co_3O_4 were 10, 21 and 30 m^2/g, respectively. The specific surface areas of all three prepared materials were larger than the commercial Co_3O_4, which had a BET surface area of only 4 m^2/g. The total pore volumes increased with increasing BET surface area and were similarly related to the Co_3O_4 morphologies. Of the prepared Co_3O_4, the cabbage-like morphology had the highest specific surface area and the total pore volume, which may be attributed to its multiple layered composite structure.

3.2. Effect of different Co_3O_4 morphologies on the degradation of 1,2,4-TrCB

The effect of the different Co_3O_4 morphologies on the degradation of 1,2,4-TrCB was evaluated at three different reaction temperatures, as shown in Fig. 3. The 1,2,4-TrCB was barely degraded with or without any of the Co_3O_4 materials at 200 °C. As the reaction temperature increased, the degradation efficiency also increased. When the reaction temperature was 300 °C, there was considerable degradation of 1,2,4-TrCB in the presence of all four types of Co_3O_4, but there was very little degradation of 1,2,4-TrCB without any Co_3O_4 present. This indicates that all four types of Co_3O_4 can promote the degradation of 1,2,4-TrCB. The reaction activities of the Co_3O_4 morphologies under different reaction temperatures consistently adhered to the following order: cabbage-like Co_3O_4 > plate-like Co_3O_4 > sphere-like Co_3O_4 > commercial Co_3O_4. The reactivity of materials is significantly dependent on their structural properties, as determined by the morphological structure [36–40]. Wang et al. reported that the increase of the specific surface area on Co_3O_4 can weaken the bond strength of Co-O, and promote more lattice oxygen desorption from Co_3O_4 to cause the reduction become easy [41]. Eiji et al. reported that catalysts with high BET surface area and high pore volume may increase their activity [42]. Table 1 shows that the pore structure parameters were different among those materials. The cabbage-like Co_3O_4 consistently exhibited a higher activity, which may be attributed to its larger specific surface area and total pore volume determined by its morphological structure, leading to more active sites on the surface of this material.

Table 1
Pore structure parameters of different materials.

Material	S_{BET} (m^2/g)	Total pore volume (cm^3/g)
Commercial Co_3O_4	4	0.043
Sphere-like Co_3O_4	10	0.062
Plate-like Co_3O_4	21	0.090
Cabbage-like Co_3O_4	30	0.140

3.3. Effect of cabbage-like Co_3O_4 dosage on the degradation of 1,2,4-TrCB and hydrodechlorination mechanism hypothesis

The cabbage-like Co_3O_4 exhibited a higher degradation activity, so a series of experiments with that material was designed to determine the effect of its dosage on 1,2,4-TrCB degradation. The dosage-dependent degradation efficiency is shown in Fig. 4(a). As the dosage of the cabbage-like Co_3O_4 increased, the amount of 1,2,4-TrCB degradation also increased. When the dosage of the cabbage-like Co_3O_4 was 350 mg, the degradation efficiency was 97.9%. Under similar experimental conditions, the degradation efficiency of 1,2,4-TrCB on used cabbage-like Co_3O_4 without further treatment still reached 91.8%. These results indicate that the reactivity of the cabbage-like Co_3O_4 on 1,2,4-TrCB degradation is promising.

Fig. 4(b) shows the effect of the cabbage-like Co_3O_4 dosage on the distribution of the less chlorinated benzenes produced during the degradation of 1,2,4-TrCB. Monochlorobenzene (MCB), *meta*-dichlorobenzene (*m*-DCB), *para*-dichlorobenzene (*p*-DCB), and *ortho*-dichlorobenzene (*o*-DCB) were identified as degradation products after GC–MS analysis, as shown in Fig. S2 of the Supplementary Material. As the dosage of cabbage-like Co_3O_4 was increased, the yield of the three DCBs and MCB initially increased, and then began to decrease. This trend indicates that a stepwise hydrodechlorination process was occurring. One chlorine atom is initially removed from 1,2,4-TrCB to form DCB, and then DCB is further dechlorinated to form MCB. A similar successive

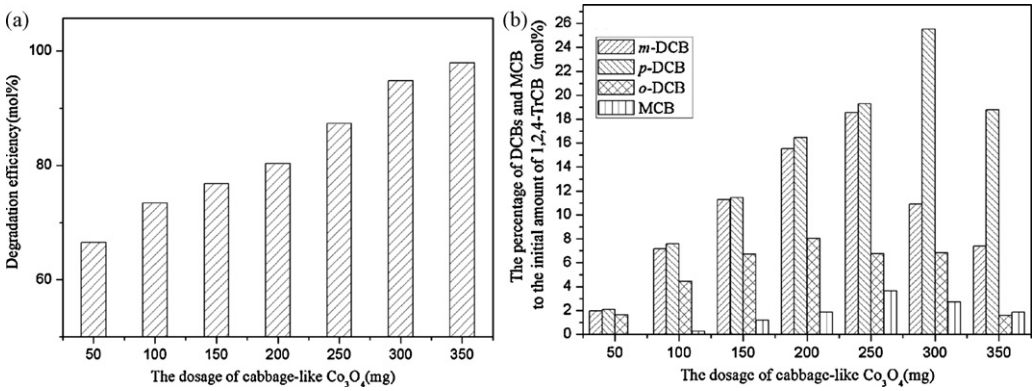

Fig. 4. (a) Effect of cabbage-like Co_3O_4 dosage on the degradation efficiencies of 1,2,4-TrCB; (b) distribution of less chlorinated benzenes formed during the degradation of 1,2,4-TrCB over different dosages of cabbage-like Co_3O_4.

hydrodechlorination pathway has been reported for the degradation of HCB by iron oxide or by UV irradiation [17,43].

It is interesting to note that the yields of the three DCBs were not equal, with *p*-DCB > *m*-DCB > *o*-DCB. Thus, it could be concluded that the difficulty in removing the chlorine atoms from 1,2,4-TrCB varied, with difficulties of Cl(4) > Cl(1) > Cl(2). However, in contrast to this result, Xu and co-workers reported that, due to the prevailing steric effect, the chlorine release from 1,2,4-TrCB over a supported nickel catalyst was fastest at the *p*-position and slowest at the *o*-position, leading to relative yields of *o*-DCB > *m*-DCB > *p*-DCB [44]. Therefore, an alternative driving force may play a crucial role in the dechlorination of 1,2,4-TrCB on the cabbage-like Co_3O_4.

Density functional theory (DFT) can be used to analyze reaction mechanisms [43]. Fueno et al. reported theoretical analyses of the dechlorination reactions of dioxins using DFT methods [45]. To investigate the discrepancy between the experimental yields of the three DCBs, the C–Cl BDEs in 1,2,4-TrCB and DCBs were calculated using the DFT method at the B3LYP/6-311++G** theory level using the Gaussian 03 program, as shown in Table 2. For 1,2,4-TrCB, the bond dissociation energy of C–Cl(2) is the lowest, and that of C–Cl(4) is the largest. This implies C–Cl(2) will be cleaved more easily than C–Cl(1), and C–Cl(4), meaning that the *p*-DCB formation is the easiest. For DCBs, the C–Cl BDE in *p*-DCB is the largest, and that in *o*-DCB is the lowest, and the energy difference of single molecule relative to *p*-DCB between *p*-DCB or *m*-DCB and *o*-DCB is about 10 kJ mol^{-1}, meaning that *p*-DCB and *m*-DCB are more stable than *o*-DCB. Thus the degradation of *p*-DCB to MCB is the most difficult, while the degradation of *o*-DCB to MCB is the easiest. The yields of the various DCBs depend on the rates of production and consumption of these compounds. The relative amounts of the three DCBs formed during the degradation process were in the order of *p*-DCB > *m*-DCB > *o*-DCB, possibly due to the BDEs described above.

Fig. 5 shows the hydrodechlorination pathway of 1,2,4-TrCB on the synthesized cabbage-like Co_3O_4. The major and minor hydrodechlorination pathways were determined by the amount of the intermediates identified during the degradation process [43]. Because of the yield of *p*-DCB was largest of the three DCBs, the dechlorination of 1,2,4-TrCB into *p*-DCB and then into MCB may be the major pathway. The theoretical calculation of C–Cl BDEs in 1,2,4-TrCB indicate that *p*-DCB will be formed most easily, and thus the conversion of 1,2,4-TrCB into *p*-DCB may be the easiest first dechlorination step, kinetically. However, the C–Cl BDEs in the three DCBs indicate that *p*-DCB is the most stable, and thus the conversion of *p*-DCB into MCB may be the hardest second dechlorination step, kinetically. In contrast, the small proportion of *o*-DCB indicates that the dechlorination of 1,2,4-TrCB into MCB via *o*-DCB, may be the minor pathway. The C–Cl BDEs for 1,2,4-TrCB and DCBs indicate that the conversion of 1,2,4-TrCB into *o*-DCB may be the hardest first dechlorination step, kinetically, while the conversion of *o*-DCB into MCB may be the easiest second dechlorination step, kinetically.

3.4. Chlorine atom distribution and TOC analysis of the decomposed products

The amounts of the DCBs and MCB are relatively low compared to the initial amount of 1,2,4-TrCB, and there is a mass imbalance between the amounts of the initial and dechlorinated materials. Table 3 shows the chlorine atom distribution among the decomposition products after reaction with 250 mg of cabbage-like Co_3O_4 at 300 °C for 60 min. The percentage of chlorine atoms in DCBs, MCB and residual 1,2,4-TrCB were 29.7%, 1.2% and 12.7%, respectively. The amount of inorganic Cl^- produced in the degradation process was determined by ion chromatograph to be 26.8%. These sources

Table 2
Calculated C–Cl bond dissociation energies in 1,2,4-TrCB and the DCBs, and the energy difference of the single molecule relative to *p*-DCB (B3LYP/6-311++G**).

Chemical	Bond	Theoretical BDE (kJ mol^{-1})	Energy difference relative to *p*-DCB (kJ mol^{-1})
(1) 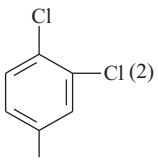	C–Cl(1)	373.71	–
Cl	C–Cl(2)	370.98	–
(4)	C–Cl(4)	378.33	–
p-DCB	C–Cl	380.82	0
m-DCB	C–Cl	377.81	0.16
o-DCB	C–Cl	373.00	10.37

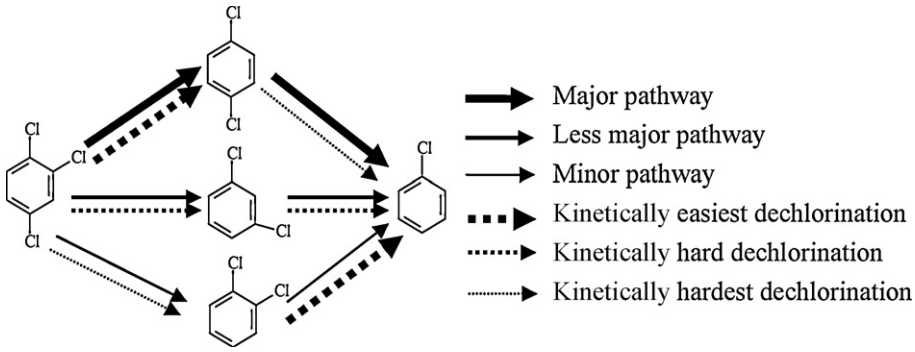

Fig. 5. Hydrodechlorination pathway for 1,2,4-TrCB degradation over cabbage-like Co_3O_4.

Table 3
Chlorine atom distribution in the degraded products.

Dechlorinated products	1,2,4-TrCB (residual)	DCBs	MCB	Cl^- (inorganic)	Other chlorinated compounds
Percentage of Cl (%)	12.7	29.7	1.2	26.8	29.6

of chlorine atoms combined account for only 70.4% of the initial chlorine atoms, leaving 29.6% of the chlorine atoms unaccounted for. A similar mass discrepancy was reported for the degradation of HCB over CaO/Fe_2O_3 and for the degradation of dioxin over alumina support [34,46,47].

TOC was also monitored to obtain information about the carbon mass balance during the degradation of 1,2,4-TrCB. The results show that the TOC of a sample of 1,2,4-TrCB reacted with 100 mg cabbage-like Co_3O_4 at 300 °C for 60 min accounted for only 57% of the TOC in the unreacted sample. About 43% of TOC was mineralized into the inorganic compounds such as CO_2 [48].

The chlorine atom and TOC results indicate that other degradation pathways, in addition to hydrodechlorination, may also occur during the degradation process.

3.5. Derivatization analysis

The other degradation pathway may be related to the oxidative degradation of 1,2,4-TrCB over the cabbage-like Co_3O_4. Amiridis et al. reported the formation of chlorophenolate via nucleophilic attack by O^{2-} on dichlorobenzene adsorbed onto V_2O_5/TiO_2 [15]. Zhang et al. confirmed the presence of pentachlorophenolate during the degradation of hexachlorobenzene over ultrafine γ-Al_2O_3 [12]. The oxygen species in Co_3O_4 are very mobile, so they may be easily utilized in oxidation reactions [20].

It was hypothesized that phenolate species could be formed during the degradation of 1,2,4-TrCB on the cabbage-like Co_3O_4. To verify this hypothesis, the products of a reaction between 1.5 μL 1,2,4-TrCB and 100 mg cabbage-like Co_3O_4 at 300 °C for 60 min were derivatized in water with acetic anhydride prior to GC–MS analysis, the results of which are shown in Fig. S3. The peaks were identified as chlorophenylacetate and dichlorophenylacetate, the derivatized products of chlorophenol and dichlorophenol, by the NIST02.L standard spectral database. These results imply that chlorophenol and dichlorophenol were formed as partial oxidation products during the degradation of 1,2,4-TrCB. Although the substitution pattern of the chlorophenol and dichlorophenol isomers could not be identified under the analytical conditions, the amounts of chlorophenol and dichlorophenol were very minor, and they are estimated to account for less than 1% of the initial chlorine atoms.

3.6. ESR analysis

ROS such as $O_2^{-\bullet}$ and $^\bullet OH$ are strong electrophilic oxidants, which can oxidize organic compounds to smaller molecular intermediates or to CO_2 and H_2O [20,21]. Their roles in a range of photocatalytic oxidative degradation reactions, including pathogenic bacteria over $NiO/SrBi_2O_4$ [49], rhodamine B over TiO_2 [50], and azodyes over $Ag/AgBr/TiO_2$ [51], have been confirmed by ESR. To identify whether 1,2,4-TrCB was decomposed by $O_2^{-\bullet}$ or $^\bullet OH$ over the cabbage-like Co_3O_4, the ESR technique, using DMPO as the spin trapping agent, was used to obtain information on the active radicals involved.

The superoxide anions were measured first. A reaction was carried out between 100 mg cabbage-like Co_3O_4 and 1.5 μL 1,2,4-TrCB at 300 °C for 60 min, and the reaction products were immediately dissolved in DMSO, then characterized by an ESR analyzer, with the results shown in Fig. 6(a). Six characteristic peaks were observed, and the hyperfine constants of $\alpha_N = 12.7429$ G, $\alpha_H = 10.0304$ G and $g = 2.0103$, coincided with those identified previously as DMPO-$O_2^{-\bullet}$ [49–53]. No $O_2^{-\bullet}$ signal was detected when pure cabbage-like Co_3O_4 was analyzed. The DMPO-$^\bullet OH$ species were measured under identical conditions except that water was used as the solvent instead of DMSO. No obvious signal was observed, as shown in Fig. 6(b). This differs from the photocatalytic degradation of many organic molecules where $^\bullet OH$ species are often identified [49–51].

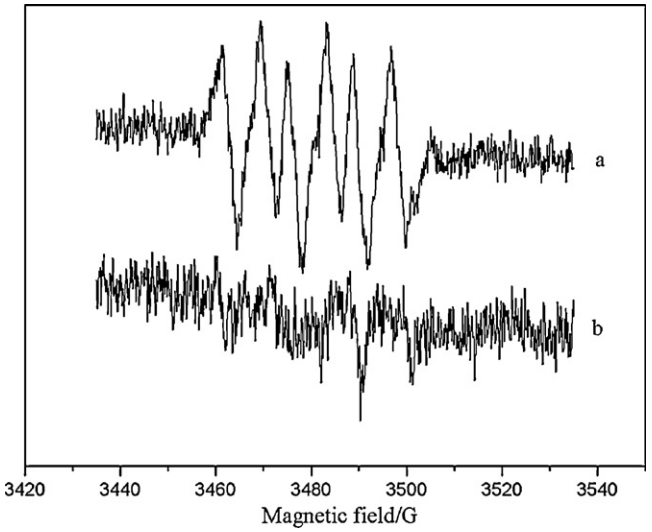

Fig. 6. ESR spectra of (a) $O_2^{-\bullet}$ and (b) $^\bullet OH$ generated after reacting 100 mg cabbage-like Co_3O_4 with 1.5 μL TrCB at 300 °C for 60 min.

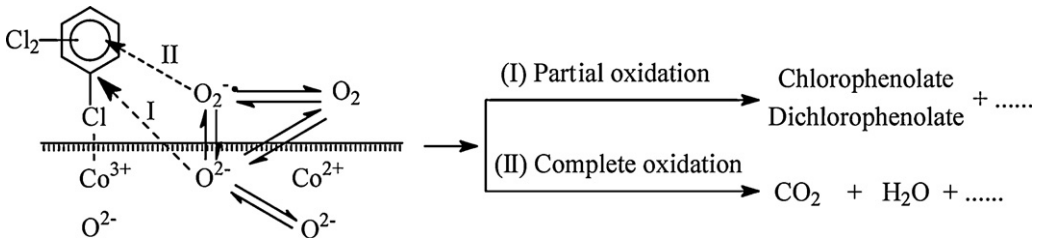

Fig. 7. Oxidative attack mechanism for 1,2,4-TrCB degradation over cabbage-like Co_3O_4.

The ESR results shown in Fig. 6 identify that the superoxide anion may be involved in the degradation of 1,2,4-TrCB, causing the ring-cracking oxidation of 1,2,4-TrCB into smaller molecular intermediates and perhaps even into CO_2 and H_2O. This may explain the mass imbalance in the chlorine atoms and TOC between the initial and degraded materials. The formation of electrophilic oxygen ions on p-type Co_3O_4 was identified by Bielanski and Haber using an ESR analyzer [54]. Additionally, the existence of O_2^{-}•, as observed directly in this experiment, supports the hypothesis of Shu and co-workers that O_2^{-}• may have an important role in the oxidative degradation of phenol over Co_3O_4 nanorods [20].

3.7. Oxidative attack degradation pathway

As described above, hydrodechlorination occurred during the degradation of 1,2,4-TrCB over cabbage-like Co_3O_4. However, there was a clear discrepancy in the mass balance of chlorine atoms and TOC between the starting and degraded materials. Thus, it must be concluded that the hydrodechlorination reaction is not the only pathway by which 1,2,4-TrCB is decomposed over cabbage-like Co_3O_4. From the results of the derivatization and ESR analysis, we propose that degradation involving oxygen attack may also occur via one of two possible pathways during the degradation process, as shown in Fig. 7.

The first reaction pathway, involving the formation of chlorophenolate and dichlorophenolate, is similar to the Mars Van Krevelen mechanism. Dissociative adsorption of the 1,2,4-TrCB occurs on the central cobalt cations. The nucleophilic lattice oxygen ions (O^{2-}) then react with the carbon associated with the C–Cl bond. The C–Cl bond is cleaved, and a Co–Cl bond is formed, resulting in the formation of chlorophenolate and dichlorophenolate as partial oxidation products. When the nearby lattice oxygen is consumed, it can be supplemented by oxygen anions transferred from surrounding cobalt cations, and the dissociated oxygen becomes lattice oxygen. Similar reaction routes have been reported for the formation of phenolates during the degradation of HCB over Al_2O_3 [12], and the degradation of chlorobenzene over iron and titanium oxide catalysts [55].

The ESR results indicate that the superoxide ion (O_2^{-}•) is one of the most important ROS on the surface of the cabbage-like Co_3O_4, and can be formed from lattice oxygen and gaseous oxygen. This superoxide ion can attack the electron cloud of the π bond in the dissociatively adsorbed 1,2,4-TrCB, and thus lead to cracking of the benzene ring into low molecular weight products and even into CO_2 and H_2O. This process may explain the mass imbalance of chlorine atoms and TOC. The details of this mechanism are shown in route II of Fig. 7.

4. Conclusions

Co_3O_4 was synthesized with three different morphologies, which were characterized as sphere-like, plate-like and cabbage-like. The effect of these different morphologies on the degradation of 1,2,4-TrCB was evaluated. The reactivity of the different Co_3O_4 morphologies had the following order: cabbage-like Co_3O_4 > plate-like Co_3O_4 > sphere-like Co_3O_4, all of which were more reactive than the commercial Co_3O_4. The differences in reactivity may be attributed to the different structural properties associated with the different morphologies of Co_3O_4. The activity of the cabbage-like Co_3O_4 for the degradation of 1,2,4-TrCB is especially promising.

Analysis of the reaction products, derivatization results, TOC analysis and ESR results suggests that both hydrodechlorination and oxygen-attacking pathways may occur competitively on the cabbage-like Co_3O_4. During the hydrodechlorination process, 1,2,4-TrCB was successively dechlorinated to form DCBs and then MCB. The yields of the three DCBs were in the order of *p*-DCB > *m*-DCB > *o*-DCB. This order can be explained by the calculated C–Cl BDEs in 1,2,4-TrCB and the DCBs. The derivatization and ESR experiments identified that the oxidation process could occur by two pathways: one pathway involves the nucleophilic lattice oxygens reacting with the carbon in the C–Cl bond, resulting in the formation of partial oxidation products such as dichlorophenolate and chlorophenolate; the other pathway involves a superoxide ion attacking the electron cloud of the π bonds in the benzene ring, leading to a comparatively complete oxidation, which may explain the mass imbalance in the chlorine atoms and TOC.

Acknowledgements

This study was supported by the Chinese Academy of Sciences (Grant No. KZCX2-YW-QN407), the National Natural Science Foundation of China (20921063, 20807049, 51078346), and the National 973 program (2009CB421606).

Appendix A. Supplementary data

Supplementary data associated with this article can be found, in the online version, at doi:10.1016/j.jhazmat.2011.07.008.

References

[1] Y.W. He, S. Tieheng, O. Ziqing, Y. Ayfer, K. Antonius, Fate of 1,2,4-trichlorobenzene (1,2,4-TCB) in soil-rice paddy system , Chemosphere 32 (1996) 1381–1389.
[2] J.Y. Zhang, W. Zhao, J. Pan, L.M. Qiu, Y.M. Zhu, Tissue-dependent distribution and accumulation of chlorobenzenes by vegetables in urban area , Environ. Int. 31 (2005) 855–860.
[3] D. Jaime, R. Manuel, D. Mario, 1,2,4-trichlorobenzene flow characteristics in saturated homogeneous and stratified porous media , Water Air Soil Pollut. 177 (2006) 3–17.
[4] K.A. Golden, C.S. Wong, J.D. Jeremiason, S.J. Eisenreich, G. Sanders, J. Hallgren, D.L. Swackhamer, D.R. Engstrom, D.T. Long, Accumulation and preliminary inventory of organochlorines in Great Lakes sediments , Water Sci. Technol. 28 (1993) 19–31.
[5] S. Fetzner, Bacterial dehalogenation , Appl. Microbiol. Biotechnol. 50 (1998) 633–657.
[6] M. Taralunga, J. Mijoin, P. Magnoux, Catalytic destruction of chlorinated POPs—catalytic oxidation of chlorobenzene over PtHFAU catalysts , Appl. Catal. B: Environ. 60 (2005) 163–171.
[7] D.F. Ollis, E. Pelizzetti, N. Serpone, Photocatalyzed destruction of water contaminants , Environ. Sci. Technol. 25 (1991) 1522–1529.

[8] G.A. Zacheis, K.A. Gray, P.V. Kamat, Radiation induced catalytic dechlorination of hexachlorobenzene on oxide surfaces , J. Phys. Chem. B 105 (2001) 4715–4720.
[9] A.K. Hall, J.M. Harrowfield, R.J. Hart, P.G. McCormick, Mechanochemical reaction of DDT with calcium oxide , Environ. Sci. Technol. 30 (1996) 3401–3407.
[10] X. Zhang, P.E. Savage, Fast catalytic oxidation of phenol in supercritical water , Catal. Today 40 (1998) 333–342.
[11] M.K. Jia, G.J. Su, M.H. Zheng, B. Zhang, S.J. Lin, Synthesis of a magnetic micro/nano Fe_xO_y-CeO_2 composite and its application for degradation of hexachlorobenzene , Sci. Chin. Chem. 53 (2010) 1266–1272.
[12] L. Zhang, M. Zheng, W. Liu, B. Zhang, G. Su, A method for decomposition of hexachlorobenzene by γ-alumina , J. Hazard. Mater. 150 (2008) 831–834.
[13] G. Schetter, R. Horch, H. Stuetzle, B.H. Hagenmaier, Low temperature thermal treatment of filter ash from municipal waste incinerators for dioxin decomposition on a technical scale , Organohalogen Compd. 3 (1990) 165–168.
[14] T. Öberg, B. Bergbäck, M. Filipsson, Catalytic effects by metal oxides on the formation and degradation of chlorinated aromatic compounds in fly ash , Chemosphere 71 (2008) 1135–1143.
[15] J. Lichtenberger, M.D. Amiridis, Catalytic oxidation of chlorinated benzenes over V_2O_5/TiO_2 catalysts , J. Catal. 223 (2004) 296–308.
[16] L. Zhang, M. Zheng, B. Zhang, W. Liu, L. Gao, T. Ba, Z. Ren, G. Su, Decomposition of hexachlorobenzene over Al_2O_3 supported metal oxide catalysts , J. Environ. Sci. 20 (2008) 1523–1526.
[17] M. Jia, G. Su, M. Zheng, B. Zhang, S. Lin, Development of self-assembled 3D FexOy micro/nano materials for application in hexachlorobenzene degradation , J. Nanosci. Nanotechnol. 11 (2011) 2100–2106.
[18] X. Ma, H. Sun, H. He, M. Zheng, Competitive reaction during decomposition of hexachlorobenzene over ultrafine Ca–Fe composite oxide catalyst , Catal. Lett. 119 (2007) 142–147.
[19] S. Krishnamoorthy, J.A. Rivas, M.D. Amiridis, Catalytic oxidation of 1,2-dichlorobenzene over supported transition metal oxides , J. Catal. 193 (2000) 264–272.
[20] T.L. Lai, Y.L. Lai, C.C. Lee, Y.Y. Shu, C.B. Wang, Microwave-assisted rapid fabrication of Co_3O_4 nanorods and application to the degradation of phenol , Catal. Today 131 (2008) 105–110.
[21] M.R. Hoffmann, S.T. Martin, W. Choi, D.W. Bahnemann, Environmental applications of semiconductor photocatalysis , Chem. Rev. 95 (1995) 69–96.
[22] Y.J. Mergler, J. Hoebink, B.E. Nieuwenhuys, CO oxidation over a $Pt/CoOx/SiO_2$ catalyst: a study using temporal analysis of products , J. Catal. 167 (1997) 305–313.
[23] J. Jansson, Low-temperature CO oxidation over Co_3O_4/Al_2O_3 , J. Catal. 194 (2000) 55–60.
[24] T. He, D. Chen, X. Jiao, Y. Xu, Y. Gu, Surfactant-assisted solvothermal synthesis of Co_3O_4 hollow spheres with oriented-aggregation nanostructures and tunable particle size , Langmuir 20 (2004) 8404–8408.
[25] Y. Jiang, Y. Wu, B. Xie, Y. Xie, Y. Qian, Moderate temperature synthesis of nanocrystalline Co_3O_4 via gel hydrothermal oxidation , Mater. Chem. Phys. 74 (2002) 234–237.
[26] S. King, K. Hyunh, R. Tannenbaum, Kinetics of nucleation, growth, and stabilization of cobalt oxide nanoclusters , J. Phys. Chem. B 107 (2003) 12097–12104.
[27] B.B. Lakshmi, C.J. Patrissi, C.R. Martin, Sol-gel template synthesis of semiconductor oxide micro- and nanostructures , Chem. Mater. 9 (1997) 2544–2550.
[28] J. Feng, H.C. Zeng, Size-controlled growth of Co_3O_4 nanocubes , Chem. Mater. 15 (2003) 2829–2835.
[29] L.S. Zhong, J.S. Hu, H.P. Liang, A.M. Cao, W.G. Song, L.J. Wan, Self-assembled 3D flowerlike iron oxide nanostructures and their application in water treatment , Adv. Mater. 18 (2006) 2426–2431.
[30] L.S. Zhong, J.S. Hu, A.M. Cao, Q. Liu, W.G. Song, L.J. Wan, 3D flowerlike ceria micro/nanocomposite structure and its application for water treatment and CO removal , Chem. Mater. 19 (2007) 1648–1655.
[31] A.M. Cao, J.D. Monnell, C. Matranga, J.M. Wu, L.L. Cao, D. Gao, Hierarchical nanostructured copper oxide and its application in arsenic removal , J. Phys. Chem. C 111 (2007) 18624–18628.
[32] S.W. Bain, Z. Ma, Z.M. Cui, L.S. Zhang, F. Niu, W.G. Song, Synthesis of micrometer-sized nanostructured magnesium oxide and its high catalytic activity in the Clainsen-Schmidt condensation reaction , J. Phys. Chem. C 112 (2008) 11340–11344.
[33] A.M. Cao, J.S. Hu, H.P. Liang, W.G. Song, L.J. Wan, X.L. He, X.G. Gao, S.H. Xia, Hierarchically structured tricobalt tetraoxide (Co_3O_4): the morphology control and its potential in sensors , J. Phys. Chem. B 110 (2006) 15858–15863.
[34] X. Ma, M. Zheng, W. Liu, Y. Qian, X. Zhao, B. Zhang, Synergic effect of calcium oxide and iron(III)oxide on the dechlorination of hexachlorobenzene , Chemosphere 60 (2005) 796–801.
[35] P. Wang, Q. Zhang, Y. Wang, T. Wang, X. Li, Y. Li, L. Ding, G. Jiang, Altitude dependence of polychlorinated biphenyls (PCBs) and polybrominated diphenyl ethers (PBDEs) in surface soil from Tibetan Plateau, China , Chemosphere 76 (2009) 1498–1504.
[36] A.K. Muzafar, N.A.M. Barakat, F.A. Sheikh, W. Baek, M.S. Khi, H.Y. Kim, Effects of silver content and morphology on the catalytic activity of silver-grafted titanium oxide nanostructure , Fiber Polym. 11 (2010) 700–709.
[37] Q. Liu, L.C. Wang, M. Chen, Y.M. Liu, Y. Cao, H.Y. He, K.N. Fan, Waste-free soft reactive grinding synthesis of high-surface-area copper–manganese spinel oxide catalysts highly effective for methanol steam reforming , Catal. Lett. 121 (2008) 144–150.
[38] F. Paolo, K. Jan, S. Valter, G. Mauro, Redox behavior of high-surface-area Rh-, Pt-, and Pd-loaded $Ce_{0.5}Zr_{0.5}O_2$ mixed oxide , J. Catal. 182 (1999) 56–69.
[39] S.M. Chin, E. Park, M.S. Kim, J. Jeong, G.N. Bae, J. Jurng, Preparation of TiO_2 ultrafine nanopowder with large surface area and its photocatalytic activity for gaseous nitrogen oxides , Powder Technol. 206 (2011) 306–311.
[40] M.W. Xue, H. Chen, J.Z. Ge, J.Y. Shen, Preparation and characterization of thermally stable high surface area mesoporous vanadium oxides , Microporous Mesoporous Mater. 131 (2010) 37–44.
[41] C.B. Wang, C.W. Tang, S.J. Gau, S.H. Chien, Effect of the surface area of cobaltic oxide on carbon monoxide oxidation , Catal. Lett. 101 (2005) 59–63.
[42] H. Eiji, I. Eiji, E.B. Mohammad, S. Yuzo, A. Shakeel, H. Halim, Y. Toshikazu, Characterization of high surface area smectite supported cobalt oxides catalysts for hydrodesulfurization by means of TPR, TPS and ESR , Appl. Catal. A: Gen. 179 (1999) 203–216.
[43] S. Yamada, Y. Naito, M. Takada, S. Nakai, M. Hosomi, Photodegradation of hexachlorobenzene and theoretical prediction of its degradation pathways using quantum chemical calculation , Chemosphere 70 (2008) 731–736.
[44] W. Wu, J. Xu, R. Ohnishi, Complete hydrodechlorination of chlorobenzene and its derivatives over supported nickel catalysts under liquid phase conditions , Appl. Catal. B: Environ. 60 (2005) 129–137.
[45] H. Fueno, K. Tanaka, S. Sugawa, Theoretical study of the dechlorination pathways of octachlorodibenzo-p-dioxin , Chemosphere 48 (2002) 771–778.
[46] M.H. Schoonenboom, H.E. Zoetemeijer, K. Olie, Dechlorination of octachlorodibenzo-p-dioxin and octachlorobenzofuran on an alumina support , Appl. Catal. B 6 (1995) 11–20.
[47] R. Weber, K. Nagai, J. Nishino, H. Shiraishi, M. Ishida, T. Takasuga, K. Konndo, M. Hiraoka, Effects of selected metal oxides on the dechlorination and destruction of PCDD and PCDF , Chemosphere 46 (2002) 1247–1253.
[48] Y. Nie, C. Hu, L. Zhou, J. Qu, Q. Wei, D. Wang, Degradation characteristics of humic acid over iron oxides/Fe0 core–shell nanoparticles with UVA/H_2O_2 , J. Hazard. Mater. 173 (2010) 474–479.
[49] C. Hu, X. Hu, J. Guo, J. Qu, Efficient destruction of pathogenic bacteria with $NiO/SrBi_2O_4$ under visible light irradiation , Environ. Sci. Technol. 40 (2006) 5508–5513.
[50] J. Zhao, T. Wu, K. Wu, K. Oikawa, H. Hidaka, N. Serpone, Photoassisted degradation of. dye pollutants. 3. Degradation of the cationic dye rhodamine B in aqueous anionic surfactant/TiO_2 dispersions under visible light irradiation: evidence for the need of substrate adsorption on TiO_2 particles , Environ. Sci. Technol. 32 (1998) 2394–2400.
[51] C. Hu, Y. Lan, J. Qu, X. Hu, A. Wang, $Ag/AgBr/TiO_2$ visible light photocatalyst for destruction of azo dyes and bacteria , J. Phys. Chem. B 110 (2006) 4066–4072.
[52] V. Brezova, A. Stasko, Spin trap study of hydroxyl radicals formed in the photocatalytic system TiO_2-water-p-cresol-oxygen , J. Catal. 14 (1994) 156–162.
[53] R. Konaka, E. Kasahara, W.C. Dunlap, Y. Yamamoto, K.C. Chien, M. Inoue, Irradiation titanium dioxide generates both singlet oxygen and superoxide anion , Free Radic. Biol. Med. 27 (1999) 294–300.
[54] A. Bielanski, J. Haber, Oxygen in catalysis on transition metal oxides , Catal. Rev. Sci. Eng. 19 (1979) 1–41.
[55] A. Khaleel, A. Al-Nayli, Supported and mixed oxide catalysts based on iron and titanium for the oxidative decomposition of chlorobenzene , Appl. Catal. B. Environ. 80 (2008) 176–184.